

Geometric Tracking Control of Omnidirectional Multirotors for Aggressive Maneuvers

Hyungyu Lee, Sheng Cheng, Zhuohuan Wu, Jaeyoung Lim, Roland Siegwart, and Naira Hovakimyan

Abstract—An omnidirectional multirotor has the maneuverability of decoupled translational and rotational motions, superseding the traditional multirotors’ motion capability. Such maneuverability is achieved due to the ability of the omnidirectional multirotor to frequently alter the thrust amplitude and direction. In doing so, the rotors’ settling time, which is induced by inherent rotor dynamics, significantly affects the omnidirectional multirotor’s tracking performance, especially in aggressive flights. To resolve this issue, we propose a novel tracking controller that takes the rotor dynamics into account and does not require additional rotor state measurement. We prove that the proposed controller yields almost global exponential stability. The proposed controller is validated in experiments, where we demonstrate significantly improved tracking performance in multiple aggressive maneuvers compared with a baseline geometric PD controller.

SUPPLEMENTARY INFORMATION

Video: <https://youtu.be/el9hllYO9r8>

I. INTRODUCTION

Multirotor vehicles, also referred to as multirotors, are becoming widely used technologies in real-world applications for their simple mechanical structure, agility, and low cost. As multirotors are brought to new application domains, there is a rising demand to further extend their maneuverability [1–4]. To fulfill this need, fully-actuated multirotors have been considered using fixed-tilt [5, 6] or variable-tilt [7, 8] rotor systems that enable the vehicle to carry out translational motions without altering the attitude. While improving maneuverability, these platforms do not show significant attitude-changing capability, such as tilting over 30 degrees during hovering. To address this issue, omnidirectional multirotors that can generate thrust to cancel out their gravity at any attitude are gaining more attention [9]. A summary of recent research on omnidirectional multirotors is presented in Table I. The domain can be categorized as omnidirectional multirotors with unidirectional rotors [10–14] or bidirectional rotors [15–19].

The unidirectional rotors have been employed extensively since they are more accessible and have a higher power

efficiency than the bidirectional ones. Furthermore, they do not experience force exertion at low speeds, which results in reversing delay. Despite these advantages, the unidirectional rotors render the system mechanically complicated since omnidirectional flights require either at least seven fixed-tilt rotors or additional servo motors paired with each rotor to enable a variable-tilt rotor system [18]. The extra mechanical parts result in increased weight of the system and challenges in control, which is undesirable for multirotors.

On the contrary, a bidirectional rotor system is complementary to the unidirectional counterpart such that one’s advantage is the disadvantage of the other. The bidirectional rotors offer an excellent solution to mitigate the mechanical complexity by unidirectional rotors [15–19]. As bidirectional rotors can generate thrust in opposite directions, unlike unidirectional thrust, they do not require additional components to facilitate direction change or thrust aid. However, bidirectional rotors suffer from the reversing delay [10, 18], which occurs while reversing the rotor’s rotational direction.

Based on the unidirectional or bidirectional rotors, existing research mainly focuses on the optimal design and control allocation methods for omnidirectional multirotors as summarized in Table I. Although aggressive flight maneuvers are essential for improving multirotors’ operational capabilities in dynamic environments [20], previous studies have not sufficiently addressed this aspect. The omnidirectional multirotors’ aggressive motion requires the rotors to frequently and precisely change speed and even direction, which necessitates accurate control of rotors. For moderate flights, rotor dynamics can be neglected to reduce the complexity of controller design by considering the dynamics of the vehicle only. However, for aggressive flights, the rotor dynamics become significant and introduce disturbances to the vehicle’s dynamics, which can lead to substantial tracking errors or even instability. In this paper, we attempt to account for the rotor dynamics to achieve precise tracking performance of omnidirectional multirotors in aggressive flights.

We propose a novel control architecture for omnidirectional multirotors, incorporating rotor dynamics directly into the controller design without necessitating additional measurements of rotor states and providing guarantees of almost global exponential stability for the omnidirectional multirotor. Unlike existing approaches that simplify the controller design with an assumption that the rotors have fast dynamics [12, 14], we explicitly take the rotor dynamics into account for the controller design. We use a simplified rotor dynamics model and investigate the impact on the vehicle’s system dynamics by formulating the equations of

*This work is supported by National Aeronautics and Space Administration (NASA ULL) grant 80NSSC22M0070 and National Science Foundation (NSF) under the RI grant #2133656.

H. Lee, S. Cheng, Z. Wu, and N. Hovakimyan are with the Department of Mechanical Science and Engineering, University of Illinois Urbana-Champaign, USA. (email: {hyungyu2, chengs, zw24, nhovakim}@illinois.edu)

J. Lim and R. Siegwart are with the Autonomous Systems Laboratory, ETH Zürich, Switzerland. (email: {jalim, rolandsi}@ethz.ch)

TABLE I

A SURVEY OF RECENT WORK IN OMNIDIRECTIONAL MULTIROTOR CONTROLS. THE ABBREVIATIONS QUAT. AND ROT. STAND FOR QUATERNION AND ROTATION MATRIX, RESPECTIVELY.

Method	Rotor-tilt Type	Propeller Type	Rotor Dynamics	Control Strategy	Stability Guarantee
[10]	Fixed-tilt	Unidirectional	N	Geometric PID control with rot.	-
O7+ [11]	Fixed-tilt	Unidirectional	N	Geometric PID control with rot.	-
[12]	Fixed-tilt	Variable-pitch	N	Geometric PID control with rot.	Almost G.E.S.
Voliro [13]	Variable-tilt	Unidirectional	N	Nonlinear PID control with quat.	-
[14]	Variable-tilt	Unidirectional	N	LQR with integral action	L.A.S.
ODAR-6 [15]	Fixed-tilt	Bidirectional	N	Geometric PID control with rot.	-
ODAR-8 [16]	Fixed-tilt	Bidirectional	N	Geometric PID control with rot.	-
[17, 19]	Fixed-tilt	Bidirectional	N	Nonlinear PID control with quat.	-
[18]	Fixed-tilt	Bidirectional	Y	Nonlinear PID control with quat.	-
Ours	Fixed-tilt	Uni/Bidirectional	Y	Geometric PD control with rot.	Almost G.E.S.

motion that include the rotor dynamics model. Based on these complete equations of motion, we design the controller to accommodate the influence induced by the rotor dynamics. In this way, the proposed method dramatically improves the tracking performance when compared with a baseline controller (which neglects the rotor dynamics) in flight experiments.

Our contributions are summarized as follows: i) We present the first omnidirectional multirotor controller design that accounts for rotor dynamics and does not require additional rotor state measurements. Furthermore, we prove the almost global exponential stability of the proposed controller with the complete system that includes the rotor dynamics; ii) We validate the proposed controller's performance using an eight-rotor omnidirectional multirotor in experiments.

This paper is structured as follows. Section II reviews related work to this research. Section III describes the modeling of general omnidirectional multirotor dynamics. Section IV explains the proposed controller and shows the stability statement. Section V demonstrates the experiment results of the omnidirectional multirotor. Section VI summarizes the paper.

II. RELATED WORK

A. Omnidirectional multirotors with unidirectional rotors

A theoretical study on the mechanical design of omnidirectional multirotors using fixed-tilt unidirectional rotors is discussed in [10], where the authors show that at least seven unidirectional fixed-tilt rotors are required for omnidirectional flight. Follow-up work with real-world validation is shown in [11]. Another approach to achieve omnidirectionality is to combine variable pitch propellers with fixed-tilt unidirectional rotors, where the propeller's pitch angle is steered by servo motors at each rotor's shaft [12]. The authors prove the controller's almost global exponential stability (G.E.S.). In [13, 14], the authors propose to use variable-tilt unidirectional rotors for omnidirectional multirotors: design and control allocation method is first proposed in [13], and an optimal control strategy, which is robust to thrust allocation singularities and guarantees local asymptotic stability (L.A.S.), is later presented in [14].

B. Omnidirectional multirotors with bidirectional rotors

A minimum number of six bidirectional rotors is required for omnidirectional flights [18]. In [15], the authors present a novel configuration to obtain omnidirectionality with six bidirectional fixed-tilt rotors. Experimental results on an eight-rotor platform are shown in [16]. The design uses an optimization method that maximizes the wrench output in any direction. In [17], the authors present optimal designs for different numbers of rotors using a similar objective function as in [15] and constraining rotors to the locations inside a unit sphere. An eight-rotor configuration is designed for maximum efficiency. The analysis of optimal design is further extended to the platform with more rotors, and an optimization-based control allocation method considering rotor dynamics is proposed in [18]. Moreover, an energy-optimal control allocation method of the same platform is proposed in [19]. In [18], the authors indirectly deal with rotor dynamics by avoiding reversing the rotor's rotation direction whenever possible. The system's stability is not analyzed.

III. MODELING

In this section, we provide the vehicle's dynamical model, including the rigid-body dynamics, the rotor dynamics, and the propeller's aerodynamics. To simplify the modeling, the following assumptions have been made, which are commonly used in the fully-actuated or omnidirectional multirotor studies [6, 13, 14]:

- The whole platform is rigid;
- Airflow induced from one rotor does not affect other rotors, which permits constant actuation dynamic coefficients, such as lift and drag coefficient;
- The desired trajectory is smooth and differentiable;
- The force and torque outputs are attainable; in other words, there is no actuator saturation.

Since we assume that the vehicle does not move at high speed, the aerodynamics can be modeled through momentum-blade element theory [21] as follows:

$$\begin{aligned} f_i &= \mu \operatorname{sgn}(\Omega_i) \Omega_i^2, \\ \tau_i &= \kappa \operatorname{sgn}(\Omega_i) \Omega_i^2, \end{aligned} \quad (1)$$

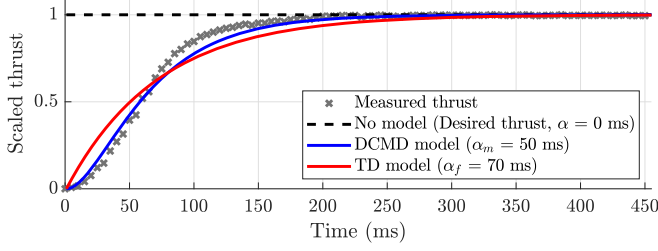


Fig. 1. Step response of a rotor with a propeller. The thrust from the rotor is scaled by the maximum thrust generated from the rotor. A 2200KV brushless rotor attached with Gemfan 513D 3-blade 3D propeller has been used for the measurement. Note that α represents the rotor time constant, and the subscripts f and m indicate the time constants of the TD and DCMD models, respectively. The desired and the no-model thrusts are the same, as the latter does not consider rotor dynamics. The time constants are determined experimentally.

$$\text{sgn}(\Omega_i) = \begin{cases} 1, & \text{if } \Omega_i \geq 0, \\ -1, & \text{if } \Omega_i < 0, \end{cases} \quad (2)$$

where $\mu \in \mathbb{R}^+$ and $\kappa \in \mathbb{R}^+$ denote the lift and drag coefficients of the rotor, respectively; $f_i \in \mathbb{R}$ and $\tau_i \in \mathbb{R}$ are the thrust force and the torque generated by the i -th rotor, respectively; and Ω_i is the angular speed of rotor i . Note that $\Omega_i \in \mathbb{R}_{\geq 0}$ holds for a unidirectional rotor, whereas $\Omega_i \in \mathbb{R}$ holds for a bidirectional rotor. The positive direction of Ω_i aligns with the z -axis of the i -th rotor as shown in Fig. 2.

There are several approaches to modeling the dynamics of a rotor [20, 22]. One frequently used approach is modeling the rotor angular speed as a first-order system using brushless DC-motor dynamics, which we refer to as the DCMD model [22]. The DCMD model fits slightly better with the measured thrust, as shown in Fig. 1. However, due to the nonlinear relationship between the thrust and rotor speed, using the DCMD model-based method introduces complexity in the controller's structure, ultimately resulting in a less practical controller.

Another approach, referred to as the thrust dynamics (TD) model, simplifies the model by treating the thrust as a first-order system [20]. The results therein show that satisfactory flight performance is preserved, although the TD model is a simplified model to ease controller design. Accordingly, as shown in Fig.1, although the DCMD model has the best performance, the TD model performs competently with no excessive errors compared to the conventional model-free method. Hence, we apply the TD model and write it as follows:

$$\dot{f}_i = \frac{1}{\alpha_i} (f_{cmd,i} - f_i), \quad (3)$$

where $f_{cmd,i} \in \mathbb{R}$ is commanded thrust, and $\alpha_i \in \mathbb{R}^+$ is the thrust time constant for the i -th rotor.

Figure 2 shows the coordinate frame of a generalized fixed-tilt omnidirectional platform. We define the global fixed frame or the inertial frame $\mathcal{F}_I = O_I, \{\hat{x}_I, \hat{y}_I, \hat{z}_I\}$, and the body frame $\mathcal{F}_B = O_B, \{\hat{x}_B, \hat{y}_B, \hat{z}_B\}$, where O_B is located at the center of mass (CoM) of the omnidirectional multirotor. We also define $\mathcal{F}_i = O_i, \{\hat{x}_i, \hat{y}_i, \hat{z}_i\}$ as the i -th

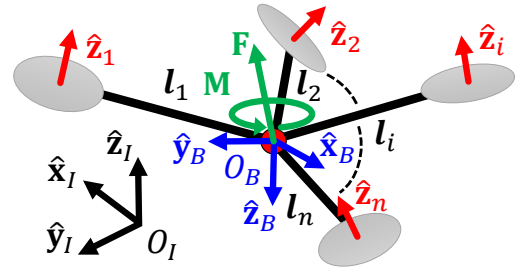


Fig. 2. Coordinate frames of a general omnidirectional multirotor, where n denotes the number of rotors and $l_i \in \mathbb{R}^3$ is the position of rotor i from O_B . Note that $n \geq 6$ should hold for bidirectional rotors and $n \geq 7$ for unidirectional ones.

rotor's frame expressed in \mathcal{F}_B .

Under the rigid-body assumption, the Newton-Euler formulation can be written as follows:

$$\dot{\mathbf{p}} = \mathbf{v}, \quad (4)$$

$$\dot{\mathbf{R}} = \mathbf{R}[\boldsymbol{\omega}]^\wedge, \quad (5)$$

$$m\dot{\mathbf{v}} = -mg\hat{z}_I + \mathbf{R}\mathbf{F}, \quad (6)$$

$$\mathbf{J}\dot{\boldsymbol{\omega}} = -\boldsymbol{\omega} \times \mathbf{J}\boldsymbol{\omega} + \mathbf{M}, \quad (7)$$

where $\mathbf{p} = [x, y, z]^T \in \mathbb{R}^3$ and $\mathbf{v} = [v_x, v_y, v_z]^T \in \mathbb{R}^3$ are the position and the linear velocity of the vehicle's CoM in the inertial frame, $\mathbf{R} \in \text{SO}(3)$ is the rotation matrix from frame \mathcal{F}_B to \mathcal{F}_I , $m \in \mathbb{R}^+$ and $\mathbf{J} \in \mathbb{R}^{3 \times 3}$ are the mass and inertial tensor of the platform, respectively, $\boldsymbol{\omega} = [\omega_x, \omega_y, \omega_z]^T \in \mathbb{R}^3$ is the angular velocity, and $\mathbf{F} = [F_x, F_y, F_z]^T \in \mathbb{R}^3$ and $\mathbf{M} = [M_x, M_y, M_z]^T \in \mathbb{R}^3$ are the force and moment applied at CoM expressed in bodyframe, respectively. Note that $\dot{\mathbf{R}} = \mathbf{R}[\boldsymbol{\omega}]^\wedge$, where $[\cdot]^\wedge : \mathbb{R}^3 \rightarrow \mathfrak{so}(3)$ is the *wedge operator* that maps a vector into a skew-symmetric matrix.

The relationship between the applied force \mathbf{F} and moment \mathbf{M} on the vehicle's body and rotor thrusts $\{f_i\}_{i=1}^n$ can be established as follows:

$$\mathbf{F} = \sum_{i=1}^n f_i \hat{z}_i, \quad \mathbf{M} = \sum_{i=1}^n (l_i \times f_i \hat{z}_i + \tau_i \hat{z}_i), \quad (8)$$

which can be expressed in the matrix form as follows:

$$\begin{bmatrix} \mathbf{F} \\ \mathbf{M} \end{bmatrix} = \mathbf{A}\mathbf{f}, \quad (9)$$

where $\mathbf{f} = [f_1, f_2, \dots, f_n]^T$ and $\mathbf{A} \in \mathbb{R}^{6 \times n}$ is the allocation matrix. Using the approximation that $\alpha_i \approx \alpha$, the single thrust dynamics model (3) can be expanded to collective wrench dynamics as follows:

$$\dot{\mathbf{w}} = \frac{1}{\alpha} (\mathbf{w}_{cmd} - \mathbf{w}), \quad (10)$$

where $\mathbf{w} = [\mathbf{F}, \mathbf{M}]^T$, $\mathbf{w}_{cmd} = [\mathbf{F}_{cmd}, \mathbf{M}_{cmd}]^T$, and \mathbf{F}_{cmd} and \mathbf{M}_{cmd} are the commanded force and moment, respectively. With (6) and (10), the vehicle's equation of motion with rotor dynamics can be established as follows:

$$m\dot{\mathbf{v}} = -\alpha\mathbf{R}\dot{\mathbf{F}} - mg\hat{z}_I + \mathbf{R}\mathbf{F}_{cmd}, \quad (11)$$

$$\mathbf{J}\dot{\boldsymbol{\omega}} = -\alpha\dot{\mathbf{M}} - \boldsymbol{\omega} \times \mathbf{J}\boldsymbol{\omega} + \mathbf{M}_{cmd}. \quad (12)$$

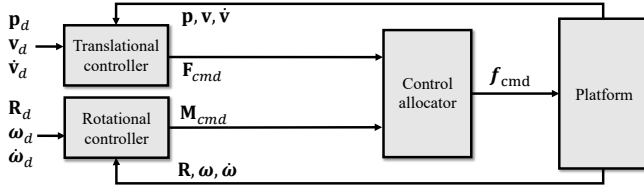


Fig. 3. The control diagram of the proposed controller.

By including rotor dynamics in the Newton-Euler equation (6) and (7), $-\alpha\mathbf{R}\dot{\mathbf{F}}$ and $-\alpha\dot{\mathbf{M}}$ appear in the equation of motion, which deteriorate the tracking performance. Note that $\dot{\mathbf{F}}$ and $\dot{\mathbf{M}}$ can be further broken down by differentiating and rearranging (6) and (7) as follows:

$$\begin{aligned}\dot{\mathbf{F}} &= \mathbf{R}^T (m\dot{\mathbf{v}} - \dot{\mathbf{R}}\mathbf{F}) = \mathbf{R}^T (m\dot{\mathbf{v}} - \mathbf{R}\hat{\boldsymbol{\omega}}\mathbf{F}) \\ &= \mathbf{R}^T m\dot{\mathbf{v}} + \mathbf{F} \times \boldsymbol{\omega},\end{aligned}\quad (13)$$

$$\dot{\mathbf{M}} = \dot{\boldsymbol{\omega}} \times \mathbf{J}\boldsymbol{\omega} + \boldsymbol{\omega} \times \mathbf{J}\dot{\boldsymbol{\omega}} + \mathbf{J}\ddot{\boldsymbol{\omega}}. \quad (14)$$

Using the results of (13) and (14), the complete equation of motion considering the effect of rotor dynamics can be written as follows:

$$m\dot{\mathbf{v}} = -\alpha m\ddot{\mathbf{v}} - \alpha\mathbf{R}(\mathbf{F} \times \boldsymbol{\omega}) - mg\hat{\mathbf{z}}_I + \mathbf{R}\mathbf{F}_{cmd}, \quad (15)$$

$$\mathbf{J}\dot{\boldsymbol{\omega}} = -\alpha(\dot{\boldsymbol{\omega}} \times \mathbf{J}\boldsymbol{\omega} + \boldsymbol{\omega} \times \mathbf{J}\dot{\boldsymbol{\omega}} + \mathbf{J}\ddot{\boldsymbol{\omega}}) - \boldsymbol{\omega} \times \mathbf{J}\boldsymbol{\omega} + \mathbf{M}_{cmd}. \quad (16)$$

From (15) and (16), we can conclude that the adverse effects of rotor dynamics are particularly pronounced when there are large linear and angular jerks ($\ddot{\mathbf{v}}$ and $\ddot{\boldsymbol{\omega}}$), significant misalignment between the force and angular velocity vectors (i.e., $\mathbf{F} \times \boldsymbol{\omega}$), substantial changes in the direction of the angular velocity vector ($\dot{\boldsymbol{\omega}}$), and a large rotor time constant (α), as shown in (15) and (16). Such conditions are prevalent during aggressive flight maneuvers, leading to further degradation of tracking performance if rotor dynamics are neglected. To mitigate these issues, we incorporate compensatory measures in the controller design, as detailed in Section IV.

IV. GEOMETRIC TRACKING CONTROL

In this section, we provide a control method for the omnidirectional multirotor to track the desired pose based on the modeling from Section III. Unlike conventional multirotor controllers [23, 24], tracking commands are carried out in two independent control loops since the translational and rotational dynamics are decoupled. We used a geometric PD controller, where we do not apply the integral term as it can amplify the rotor's settling time due to its integral nature. Furthermore, we define force and moment errors to take rotor dynamics into account in the controller design.

Figure 3 shows the overall control diagram of the proposed controller. The inputs $\mathbf{p}_d = [x_d, y_d, z_d]^T \in \mathbb{R}^3$, $\mathbf{v}_d = [v_{x_d}, v_{y_d}, v_{z_d}]^T \in \mathbb{R}^3$, and $\dot{\mathbf{v}}_d$ are fed to the position controller along with the actual position \mathbf{p} and velocity \mathbf{v} . Simultaneously, the inputs $\mathbf{R}_d \in \text{SO}(3)$, $\boldsymbol{\omega}_d = [\omega_{x_d}, \omega_{y_d}, \omega_{z_d}]^T \in \mathbb{R}^3$, and $\dot{\boldsymbol{\omega}}_d \in \mathbb{R}^3$ are fed to the attitude controller along with actual rotation matrix \mathbf{R} and angular

velocity $\boldsymbol{\omega}$. Outputs from position and attitude controllers, commanded force \mathbf{F}_{cmd} and moment \mathbf{M}_{cmd} , are sent to the control allocator to generate thrusts on all rotors \mathbf{f}_{cmd} by $\mathbf{f}_{cmd} = \mathbf{A}^\dagger[\mathbf{F}_{cmd}^T, \mathbf{M}_{cmd}^T]^T$, where \mathbf{A}^\dagger is pseudo-inverse matrix of allocation matrix \mathbf{A} .

A. Translational Controller

For the translational controller, we define the position error $\mathbf{e}_p = [e_x, e_y, e_z]^T \in \mathbb{R}^3$, velocity error $\mathbf{e}_v = [e_{v_x}, e_{v_y}, e_{v_z}]^T \in \mathbb{R}^3$, and force error $\mathbf{e}_F \in \mathbb{R}^3$ as follows:

$$\mathbf{e}_p = \mathbf{p} - \mathbf{p}_d, \quad (17)$$

$$\mathbf{e}_v = \mathbf{v} - \mathbf{v}_d, \quad (18)$$

$$\mathbf{e}_F = \mathbf{F} - \mathbf{F}_d, \quad (19)$$

where desired force $\mathbf{F}_d \in \mathbb{R}^3$ is defined as

$$\mathbf{F}_d = \mathbf{R}^T (-k_p \mathbf{e}_p - k_v \mathbf{e}_v + mg\hat{\mathbf{z}}_I + m\dot{\mathbf{v}}_d), \quad (20)$$

for $k_p \in \mathbb{R}^+$ and $k_v \in \mathbb{R}^+$ being position and velocity gains, respectively.

To accommodate the settling time of the generated force, the force controller is designed as follows:

$$\mathbf{F}_{cmd} = \mathbf{F}_d + \alpha\dot{\mathbf{F}}_d, \quad (21)$$

where $\dot{\mathbf{F}}_d$, obtained by differentiating equations (17), (18), and (20), can be expressed as follows:

$$\begin{aligned}\dot{\mathbf{F}}_d &= \dot{\mathbf{R}}^T (-k_p \mathbf{e}_p - k_v \mathbf{e}_v + mg\hat{\mathbf{z}}_I + m\dot{\mathbf{v}}_d) \\ &\quad + \mathbf{R}^T \frac{d}{dt} (-k_p \mathbf{e}_p - k_v \mathbf{e}_v + mg\hat{\mathbf{z}}_I + m\dot{\mathbf{v}}_d), \\ &= -[\boldsymbol{\omega}]^\wedge \mathbf{F}_d + \mathbf{R}^T \left(-k_p \mathbf{e}_v - \frac{k_v}{m} \mathbf{e}_F + m\ddot{\mathbf{v}}_d \right),\end{aligned}\quad (22)$$

$$= \mathbf{F}_d \times \boldsymbol{\omega} + \mathbf{R}^T \left(-k_p \mathbf{e}_v - \frac{k_v}{m} \mathbf{e}_F + m\ddot{\mathbf{v}}_d \right). \quad (23)$$

Applying (22) to (21), the complete form of control law can be written as:

$$\begin{aligned}\mathbf{F}_{cmd} &= \mathbf{R}^T \left(-k_p \mathbf{e}_p - (\alpha k_p + k_v) \mathbf{e}_v - \frac{\alpha k_v}{m} \mathbf{e}_F \right. \\ &\quad \left. + mg\hat{\mathbf{z}}_I + m\dot{\mathbf{v}}_d + \alpha\mathbf{R}(\mathbf{F}_d \times \boldsymbol{\omega}) + \alpha m\ddot{\mathbf{v}}_d \right).\end{aligned}\quad (24)$$

Note that $\ddot{\mathbf{v}}_d$ can be analytically computed from the given trajectory as the desired trajectory is 3rd-order and continuous. Considering that \mathbf{e}_F , which can be estimated using onboard IMU, is subject to sensor noise uncorrelated with trajectory tracking, filtering methods (such as a first-order low-pass filter) can be applied to suppress high-frequency noise. The specific parameters of the filter can be adjusted based on the application's requirements and the characteristics of the sensor noise.

B. Rotational Controller

For the rotational controller, we define the attitude error $\mathbf{e}_R = [e_{R_x}, e_{R_y}, e_{R_z}]^T \in \mathbb{R}^3$, angular velocity error $\mathbf{e}_\omega = [e_{\omega_x}, e_{\omega_y}, e_{\omega_z}]^T \in \mathbb{R}^3$, and moment error $\mathbf{e}_M \in \mathbb{R}^3$ as follows:

$$\mathbf{e}_R = \frac{[\mathbf{R}_d^T \mathbf{R} - \mathbf{R}^T \mathbf{R}_d]^\vee}{2\sqrt{1 + \text{tr}(\mathbf{R}_d^T \mathbf{R})}}, \quad (25)$$

$$\mathbf{e}_\omega = \boldsymbol{\omega} - \mathbf{R}^T \mathbf{R}_d \boldsymbol{\omega}_d, \quad (26)$$

$$\mathbf{e}_M = \mathbf{M} - \mathbf{M}_d, \quad (27)$$

where the *vee operator* $[\cdot]^\vee : \mathfrak{so}(3) \rightarrow \mathbb{R}^3$ is the inverse of the *wedge operator* and $\text{tr}(\cdot)$ is the trace of a square matrix. Note that the definition of \mathbf{e}_R is first proposed in [25] and it is mathematically equivalent to the quaternion-based attitude error [26]. The desired moment $\mathbf{M}_d \in \mathbb{R}^3$ is defined as

$$\begin{aligned} \mathbf{M}_d &= -k_R \mathbf{e}_R - k_\omega \mathbf{e}_\omega + \boldsymbol{\omega} \times \mathbf{J} \boldsymbol{\omega} \\ &\quad - \mathbf{J}([\boldsymbol{\omega}]^\wedge \mathbf{R}^T \mathbf{R}_d \boldsymbol{\omega}_d - \mathbf{R}^T \mathbf{R}_d \dot{\boldsymbol{\omega}}_d), \end{aligned} \quad (28)$$

where $k_R \in \mathbb{R}^+$ and $k_\omega \in \mathbb{R}^+$ are attitude and angular velocity gains, respectively.

To resolve the settling time of the generated moment, the moment controller is designed as follows:

$$\mathbf{M}_{cmd} = \mathbf{M}_d + \alpha \dot{\mathbf{M}}_d. \quad (29)$$

We use the following equalities in our derivation:

$$\frac{d}{dt}(\mathbf{R}^T \mathbf{R}_d) = \mathbf{R}^T \mathbf{R}_d [\boldsymbol{\omega}_d]^\wedge - [\boldsymbol{\omega}]^\wedge \mathbf{R}^T \mathbf{R}_d, \quad (30)$$

$$\frac{d}{dt}(\mathbf{R}^T \mathbf{R}_d \boldsymbol{\omega}_d) = \mathbf{R}^T \mathbf{R}_d \dot{\boldsymbol{\omega}}_d - [\boldsymbol{\omega}]^\wedge \mathbf{R}^T \mathbf{R}_d \boldsymbol{\omega}_d, \quad (31)$$

$$\begin{aligned} \frac{d}{dt}(\mathbf{R}^T \mathbf{R}_d \dot{\boldsymbol{\omega}}_d) &= \frac{d}{dt}(\mathbf{R}^T \mathbf{R}_d) \dot{\boldsymbol{\omega}}_d + \mathbf{R}^T \mathbf{R}_d \ddot{\boldsymbol{\omega}}_d \\ &= \mathbf{R}^T \mathbf{R}_d [\boldsymbol{\omega}_d]^\wedge \dot{\boldsymbol{\omega}}_d - [\boldsymbol{\omega}]^\wedge \mathbf{R}^T \mathbf{R}_d \dot{\boldsymbol{\omega}}_d + \mathbf{R}^T \mathbf{R}_d \ddot{\boldsymbol{\omega}}_d \end{aligned} \quad (32)$$

$$\begin{aligned} \frac{d}{dt}([\boldsymbol{\omega}]^\wedge \mathbf{R}^T \mathbf{R}_d \boldsymbol{\omega}_d) \\ &= [\dot{\boldsymbol{\omega}}]^\wedge \mathbf{R}^T \mathbf{R}_d \boldsymbol{\omega}_d + [\boldsymbol{\omega}]^\wedge \frac{d}{dt}(\mathbf{R}^T \mathbf{R}_d \boldsymbol{\omega}_d) \\ &= [\boldsymbol{\omega}]^\wedge \mathbf{R}^T \mathbf{R}_d \boldsymbol{\omega}_d + [\boldsymbol{\omega}]^\wedge \mathbf{R}^T \mathbf{R}_d \dot{\boldsymbol{\omega}}_d - [\boldsymbol{\omega}]^\wedge [\boldsymbol{\omega}]^\wedge \mathbf{R}^T \mathbf{R}_d \boldsymbol{\omega}_d. \end{aligned} \quad (33)$$

By differentiating (25), (26), and (28), $\dot{\mathbf{M}}_d$ can be expressed as follows:

$$\begin{aligned} \dot{\mathbf{M}}_d &= -k_R \dot{\mathbf{e}}_R - k_\omega \dot{\mathbf{e}}_\omega + \boldsymbol{\omega} \times \mathbf{J} \dot{\boldsymbol{\omega}} + \dot{\boldsymbol{\omega}} \times \mathbf{J} \boldsymbol{\omega} \\ &\quad + \mathbf{J}([\boldsymbol{\omega}]^\wedge [\boldsymbol{\omega}]^\wedge \mathbf{R}^T \mathbf{R}_d \boldsymbol{\omega}_d - [\dot{\boldsymbol{\omega}}]^\wedge \mathbf{R}^T \mathbf{R}_d \boldsymbol{\omega}_d \\ &\quad \mathbf{R}^T \mathbf{R}_d [\boldsymbol{\omega}_d]^\wedge \dot{\boldsymbol{\omega}}_d - 2[\boldsymbol{\omega}]^\wedge \mathbf{R}^T \mathbf{R}_d \dot{\boldsymbol{\omega}}_d + \mathbf{R}^T \mathbf{R}_d \ddot{\boldsymbol{\omega}}_d), \end{aligned} \quad (34)$$

where, based on [25], $\dot{\mathbf{e}}_R$ and $\dot{\mathbf{e}}_\omega$ are:

$$\dot{\mathbf{e}}_R = \frac{(\text{tr}[\mathbf{R}^T \mathbf{R}_d] \mathbf{I} - \mathbf{R}^T \mathbf{R}_d + 2\mathbf{e}_R \mathbf{e}_R^T) \mathbf{e}_\omega}{2\sqrt{1 + \text{tr}[\mathbf{R}_d^T \mathbf{R}]}} \quad (35)$$

$$\dot{\mathbf{e}}_\omega = \dot{\boldsymbol{\omega}} + [\boldsymbol{\omega}]^\wedge \mathbf{R}^T \mathbf{R}_d \boldsymbol{\omega}_d - \mathbf{R}^T \mathbf{R}_d \dot{\boldsymbol{\omega}}_d \quad (36)$$

Similar to \mathbf{e}_F , \mathbf{e}_M is subject to sensor noise that is uncorrelated with trajectory tracking, and hence filtering methods (such as a first-order low-pass filter) can be applied to suppress high-frequency noise.

C. Stability Analysis

For the stability analysis, we first analyze the stability of the translational and rotational control systems individually and then combine the results for the full system's stability.

Proposition 1: (Global exponential stability of the translational system) Consider the commanded force \mathbf{F}_{cmd} defined in (21). If the positive design constants k_p , k_v , and c_1 satisfy

$$k_p > \frac{c_1 k_v^2 + 2c_1 k_v - c_1^2}{m(4(k_v - c_1) - 1)}, \quad (37)$$

$$k_v > c_1 + \frac{1}{4}, \quad (38)$$

then the zero equilibrium of the translational tracking error dynamics of \mathbf{e}_p , \mathbf{e}_v , and \mathbf{e}_F is globally exponentially stable.

Proof: Let a Lyapunov function candidate \mathcal{V}_1 for the translational system be

$$\mathcal{V}_1 = \frac{1}{2} k_p \|\mathbf{e}_p\|^2 + \frac{1}{2} m \|\mathbf{e}_v\|^2 + \frac{1}{2} \alpha \|\mathbf{e}_F\|^2 + c_1 \mathbf{e}_p \cdot \mathbf{e}_v, \quad (39)$$

where $\|\cdot\|$ denotes the Euclidean norm.

By Cauchy-Schwartz inequality, we can show that, for k_p satisfying (37), \mathcal{V}_1 is bounded by

$$\mathbf{z}_1^T \mathbf{M}_{11} \mathbf{z}_1 \leq \mathcal{V}_1 \leq \mathbf{z}_1^T \mathbf{M}_{12} \mathbf{z}_1, \quad (40)$$

where $\mathbf{z}_1 = [\|\mathbf{e}_p\|, \|\mathbf{e}_v\|, \|\mathbf{e}_F\|]^T \in \mathbb{R}^3$, and the matrices \mathbf{M}_{11} and $\mathbf{M}_{12} \in \mathbb{R}^{3 \times 3}$ are defined as

$$\mathbf{M}_{11} = \frac{1}{2} \begin{bmatrix} k_p & -c_1 & 0 \\ -c_1 & m & 0 \\ 0 & 0 & \alpha \end{bmatrix}, \quad \mathbf{M}_{12} = \frac{1}{2} \begin{bmatrix} k_p & c_1 & 0 \\ c_1 & m & 0 \\ 0 & 0 & \alpha \end{bmatrix}.$$

Now we deal with the boundedness of $\dot{\mathcal{V}}_1$. From (10), (20), and (21), the force error dynamics can be written as

$$\begin{aligned} \alpha \dot{\mathbf{e}}_F &= \alpha \dot{\mathbf{F}} - \alpha \dot{\mathbf{F}}_d = (\mathbf{F}_{cmd} - \mathbf{F}) - \alpha \dot{\mathbf{F}}_d \\ &= (\mathbf{F}_d + \alpha \dot{\mathbf{F}}_d - \mathbf{F}) - \alpha \dot{\mathbf{F}}_d = -(\mathbf{F} - \mathbf{F}_d) \\ &= -\mathbf{e}_F. \end{aligned} \quad (41)$$

By (11), (20), (21), and (41), the velocity error dynamics can be written as

$$\begin{aligned} m \dot{\mathbf{e}}_v &= m \dot{\mathbf{v}} - m \dot{\mathbf{v}}_d = -\alpha \mathbf{R} \dot{\mathbf{F}} - mg \hat{\mathbf{z}}_1 + \mathbf{R} \mathbf{F}_{cmd} - m \dot{\mathbf{v}}_d \\ &= -k_p \mathbf{e}_p - k_v \mathbf{e}_v - \alpha \mathbf{R} (\dot{\mathbf{F}} - \dot{\mathbf{F}}_d) \\ &= -k_p \mathbf{e}_p - k_v \mathbf{e}_v + \mathbf{R} \mathbf{e}_F. \end{aligned} \quad (42)$$

Using (41)–(42), the time derivative of \mathcal{V}_1 is given by

$$\begin{aligned} \dot{\mathcal{V}}_1 &= k_p \mathbf{e}_p \cdot \mathbf{e}_v + m \mathbf{e}_v \cdot \dot{\mathbf{e}}_v + \alpha \mathbf{e}_F \cdot \dot{\mathbf{e}}_F \\ &\quad + c_1 (\dot{\mathbf{e}}_p \cdot \mathbf{e}_v + \mathbf{e}_p \cdot \dot{\mathbf{e}}_v) \\ &= k_p \mathbf{e}_p \cdot \mathbf{e}_v + \mathbf{e}_v \cdot (-k_p \mathbf{e}_p - k_v \mathbf{e}_v + \mathbf{R} \mathbf{e}_F) - \mathbf{e}_F \cdot \mathbf{e}_F \\ &\quad + c_1 \left(\dot{\mathbf{e}}_p \cdot \mathbf{e}_v + \mathbf{e}_p \cdot \frac{1}{m} (-k_p \mathbf{e}_p - k_v \mathbf{e}_v + \mathbf{R} \mathbf{e}_F) \right) \\ &= -\frac{c_1 k_p}{m} \|\mathbf{e}_p\|^2 - (k_v - c_1) \|\mathbf{e}_v\|^2 - \|\mathbf{e}_F\|^2 \\ &\quad + \frac{c_1 k_v}{m} \mathbf{e}_p \cdot \mathbf{e}_v + \mathbf{R} \mathbf{e}_F \cdot \left(\mathbf{e}_v + \frac{c_1}{m} \mathbf{e}_p \right). \end{aligned} \quad (43)$$

Since $\|\mathbf{R} \mathbf{e}_F\| = \|\mathbf{e}_F\|$ holds by the property of rotation matrix [27], we can show that $\dot{\mathcal{V}}_1$ is bounded by

$$\dot{\mathcal{V}}_1 \leq -\mathbf{z}_1^T \mathbf{W}_1 \mathbf{z}_1, \quad (44)$$

where

$$\mathbf{W}_1 = \begin{bmatrix} \frac{c_1 k_p}{m} & -\frac{c_1 k_v}{2m} & -\frac{c_1}{2m} \\ -\frac{c_1 k_v}{2m} & k_v - c_1 & -\frac{1}{2} \\ -\frac{c_1}{2m} & -\frac{1}{2} & 1 \end{bmatrix}.$$

With the positive design constants k_p , k_v , and c_1 satisfying (37) and (38), the matrices \mathbf{M}_{11} , \mathbf{M}_{12} , and \mathbf{W}_1 are always positive definite. As a result, \mathcal{V}_1 is always bounded as in (40), and $\dot{\mathcal{V}}_1$ is always negative within the region of attraction $\mathbf{z}_1 \in \mathbb{R}^3$. Thus, the translational motion of the system is globally exponentially stable [28]. ■

To show the stability of the rotational system, we first define the rotational error function between two rotation matrices, \mathbf{R}_1 and \mathbf{R}_2 , as follows:

$$\Psi(\mathbf{R}_1, \mathbf{R}_2) = 2 - \sqrt{1 + \text{tr}(\mathbf{R}_d^T \mathbf{R}_1)}. \quad (45)$$

Note that $\Psi(\mathbf{R}_1, \mathbf{R}_2)$ is bounded by $0 \leq \Psi(\mathbf{R}_1, \mathbf{R}_2) \leq 2$, and $\Psi(\mathbf{R}_1, \mathbf{R}_2) = 2$ if and only if the minimum angle required to rotate from \mathbf{R}_1 to \mathbf{R}_2 is 180 degrees.

Proposition 2: (Almost global exponential stability of the rotational system) Consider the commanded moment \mathbf{M}_{cmd} defined in (29). If the vehicle's initial rotation matrix \mathbf{R} satisfies

$$\Psi(\mathbf{R}(0), \mathbf{R}_d(0)) < 2, \quad (46)$$

and the positive design constants k_R , k_ω , and c_2 satisfy

$$k_R > \frac{c_2 k_\omega^2}{\lambda_m (4(k_\omega - \frac{1}{2}c_2) - 1)}, \quad (47)$$

$$k_\omega > \frac{1}{2}c_2 + \frac{1}{4}, \quad (48)$$

where λ_m denotes the minimum eigenvalue of the inertia tensor \mathbf{J} , then the zero equilibrium of the rotational tracking error dynamics of \mathbf{e}_R , \mathbf{e}_ω , and \mathbf{e}_M is almost globally exponentially stable.

Proof: Let a Lyapunov function candidate for rotational system \mathcal{V}_2 be

$$\mathcal{V}_2 = \frac{1}{2} \mathbf{e}_\omega \cdot \mathbf{J} \mathbf{e}_\omega + k_R \Psi(\mathbf{R}, \mathbf{R}_d) + \frac{1}{2} \alpha \|\mathbf{e}_M\|^2 + c_2 \mathbf{e}_R \cdot \mathbf{e}_\omega. \quad (49)$$

In [25], it has been shown that $\Psi(\mathbf{R}, \mathbf{R}_d)$ is bounded by

$$\|\mathbf{e}_R\|^2 \leq \Psi(\mathbf{R}, \mathbf{R}_d) \leq 2 \|\mathbf{e}_R\|^2. \quad (50)$$

Using (50) and $\lambda_m \|\mathbf{e}_\omega\|^2 \leq \mathbf{e}_\omega \cdot \mathbf{J} \mathbf{e}_\omega \leq \lambda_M \|\mathbf{e}_\omega\|^2$, where λ_M is the maximum eigenvalue of \mathbf{J} , we can show that, for k_R and k_ω satisfying (47), \mathcal{V}_2 is bounded by

$$\mathbf{z}_2^T \mathbf{M}_{21} \mathbf{z}_2 \leq \mathcal{V}_2 \leq \mathbf{z}_2^T \mathbf{M}_{22} \mathbf{z}_2, \quad (51)$$

where $\mathbf{z}_2 = [\|\mathbf{e}_R\|, \|\mathbf{e}_\omega\|, \|\mathbf{e}_M\|]^T \in \mathbb{R}^3$, and the matrices \mathbf{M}_{21} and $\mathbf{M}_{22} \in \mathbb{R}^{3 \times 3}$ are defined as

$$\mathbf{M}_{21} = \frac{1}{2} \begin{bmatrix} 2k_R & -c_2 & 0 \\ -c_2 & \lambda_m & 0 \\ 0 & 0 & \alpha \end{bmatrix}, \mathbf{M}_{22} = \frac{1}{2} \begin{bmatrix} 4k_R & c_2 & 0 \\ c_2 & \lambda_M & 0 \\ 0 & 0 & \alpha \end{bmatrix}.$$

Now we deal with the boundedness of $\dot{\mathcal{V}}_2$. In [25], it has been shown that the following relationships hold:

$$\dot{\Psi}(\mathbf{R}, \mathbf{R}_d) = \mathbf{e}_R \cdot \mathbf{e}_\omega, \quad (52)$$

$$\|\dot{\mathbf{e}}_R\| \leq \frac{1}{2} \|\mathbf{e}_\omega\|. \quad (53)$$

From (10), (28), and (29), the moment error dynamics can be written as

$$\begin{aligned} \alpha \dot{\mathbf{e}}_M &= \alpha \dot{\mathbf{M}} - \alpha \dot{\mathbf{M}}_d = (\mathbf{M}_{cmd} - \mathbf{M}) - \alpha \dot{\mathbf{M}}_d \\ &= (\mathbf{M}_d + \alpha \dot{\mathbf{M}}_d - \mathbf{M}) - \alpha \dot{\mathbf{M}}_d = -(\mathbf{M} - \mathbf{M}_d) \\ &= -\mathbf{e}_M. \end{aligned} \quad (54)$$

From (12), (28), (29), and (54), the angular velocity error dynamics can be written as

$$\begin{aligned} \mathbf{J} \dot{\mathbf{e}}_\omega &= \mathbf{J} \dot{\boldsymbol{\omega}} - \mathbf{J} \frac{d}{dt} (\mathbf{R}^T \mathbf{R}_d \boldsymbol{\omega}_d) \\ &= \mathbf{J} \dot{\boldsymbol{\omega}} + \mathbf{J} ([\boldsymbol{\omega}]^\wedge \mathbf{R}^T \mathbf{R}_d \boldsymbol{\omega}_d - \mathbf{R}^T \mathbf{R}_d \dot{\boldsymbol{\omega}}_d) \\ &= -k_R \mathbf{e}_R - k_\omega \mathbf{e}_\omega - \alpha (\dot{\mathbf{M}} - \dot{\mathbf{M}}_d) \\ &= -k_R \mathbf{e}_R - k_\omega \mathbf{e}_\omega + \mathbf{e}_M. \end{aligned} \quad (55)$$

Using (52)–(55), the time derivative of \mathcal{V}_2 is given by

$$\begin{aligned} \dot{\mathcal{V}}_2 &= \mathbf{e}_\omega \cdot \mathbf{J} \dot{\mathbf{e}}_\omega + k_R \dot{\Psi}(\mathbf{R}, \mathbf{R}_d) + \alpha \mathbf{e}_M \cdot \dot{\mathbf{e}}_M \\ &\quad + c_2 (\dot{\mathbf{e}}_R \cdot \mathbf{e}_\omega + \mathbf{e}_R \cdot \dot{\mathbf{e}}_\omega) \\ &= \mathbf{e}_\omega \cdot (-k_R \mathbf{e}_R - k_\omega \mathbf{e}_\omega + \mathbf{e}_M) + k_R \mathbf{e}_R \cdot \mathbf{e}_\omega - \mathbf{e}_M \cdot \mathbf{e}_M \\ &\quad + c_2 \dot{\mathbf{e}}_R \cdot \mathbf{e}_\omega + c_2 \mathbf{e}_R \cdot \mathbf{J}^{-1} (-k_R \mathbf{e}_R - k_\omega \mathbf{e}_\omega + \mathbf{e}_M) \\ &= -k_\omega \|\mathbf{e}_\omega\|^2 - \|\mathbf{e}_M\|^2 - c_2 k_R \mathbf{e}_R \cdot \mathbf{J}^{-1} \mathbf{e}_R + c_2 \dot{\mathbf{e}}_R \cdot \mathbf{e}_\omega \\ &\quad - c_2 k_\omega \mathbf{e}_R \cdot \mathbf{J}^{-1} \mathbf{e}_\omega + \mathbf{e}_M \cdot \mathbf{e}_\omega + c_2 \mathbf{e}_R \cdot \mathbf{J}^{-1} \mathbf{e}_M. \end{aligned} \quad (56)$$

As $\|\dot{\mathbf{e}}_R\| \leq \frac{1}{2} \|\mathbf{e}_\omega\|$, we can show that $\dot{\mathcal{V}}_2$ is bounded by

$$\dot{\mathcal{V}}_2 \leq -\mathbf{z}_2^T \mathbf{W}_2 \mathbf{z}_2, \quad (57)$$

where

$$\mathbf{W}_2 = \begin{bmatrix} \frac{c_2 k_R}{\lambda_m} & \frac{c_2 k_\omega}{2\lambda_m} & -\frac{c_2}{2\lambda_M} \\ \frac{c_2 k_\omega}{2\lambda_m} & k_\omega - \frac{1}{2}c_2 & -\frac{1}{2} \\ -\frac{c_2}{2\lambda_M} & -\frac{1}{2} & 1 \end{bmatrix}.$$

With the positive design constants k_R , k_ω , and c_2 satisfying (47) and (48), the matrices \mathbf{M}_{21} , \mathbf{M}_{22} , and \mathbf{W}_2 are always positive definite. As a result, \mathcal{V}_2 is always bounded as in (51), and $\dot{\mathcal{V}}_2$ is always negative within the region of attraction in (46). Thus, the rotational motion of the system is almost globally exponentially stable. ■

Theorem 1: (Almost global exponential stability of the full system) Consider the commanded force \mathbf{F}_{cmd} and the commanded moment \mathbf{M}_{cmd} defined in (21) and (29). If positive design constants c_1 , c_2 , k_p , k_v , k_R , and k_ω satisfy (37), (38), (47), and (48), then the zero equilibrium of the tracking error dynamics of \mathbf{e}_p , \mathbf{e}_v , \mathbf{e}_R , \mathbf{e}_ω , \mathbf{e}_F , and \mathbf{e}_M is exponentially stable.

Proof: Let a Lyapunov function candidate \mathcal{V} for the full system be

$$\mathcal{V} = \mathcal{V}_1 + \mathcal{V}_2. \quad (58)$$

Using (40) and (51), the function \mathcal{V} can be bounded

$$\mathbf{z}_1^T \mathbf{M}_{11} \mathbf{z}_1 + \mathbf{z}_2^T \mathbf{M}_{21} \mathbf{z}_2 \leq \mathcal{V} \leq \mathbf{z}_1^T \mathbf{M}_{12} \mathbf{z}_1 + \mathbf{z}_2^T \mathbf{M}_{22} \mathbf{z}_2. \quad (59)$$

From (44) and (57), the time derivative of \mathcal{V} is bounded by

$$\dot{\mathcal{V}} \leq -\mathbf{z}_1^T \mathbf{W}_1 \mathbf{z}_1 - \mathbf{z}_2^T \mathbf{W}_2 \mathbf{z}_2. \quad (60)$$

With the positive design constants satisfying (37), (38), (47), and (48), the matrices \mathbf{M}_{11} , \mathbf{M}_{12} , \mathbf{M}_{21} , \mathbf{M}_{22} , \mathbf{W}_1 , and \mathbf{W}_2 are always positive definite. As a result, \mathcal{V} is always bounded as in (59), and $\dot{\mathcal{V}}$ is always negative within the region of attraction in (46). Thus, the full system is almost globally exponentially stable, when the region of attraction is given by (46). ■

V. EXPERIMENTAL VALIDATION

In this section, we present the experimental results validating the proposed controller's performance. We compare the proposed controller with a baseline controller for tracking performance. The baseline controller has $\alpha = 0$, i.e., the rotors are ideal with no settling time, resulting in using \mathbf{F}_d and \mathbf{M}_d as control inputs. For the proposed rotational controller, we used the simplified form of \mathbf{M}_d . Note that by assuming the rotational tracking control performance is sufficiently high so that $\mathbf{R}^T \mathbf{R}_d \approx \mathbf{I}$, \mathbf{M}_d can be written in following simplified form:

$$\dot{\mathbf{M}}_d \approx -\frac{1}{2} k_R \mathbf{e}_\omega - k_\omega \mathbf{J}^{-1} \mathbf{e}_M + \boldsymbol{\omega} \times \mathbf{J} \boldsymbol{\omega} + \dot{\boldsymbol{\omega}} \times \mathbf{J} \boldsymbol{\omega} + \mathbf{J} \ddot{\boldsymbol{\omega}}.$$

For the omnidirectional multirotor platform, we used the configuration with eight fixed-tilt bidirectional rotors proposed in [17], as it has been shown to maximize the vehicle's agility while making its characteristics nearly rotationally invariant. For the platform's main electrical components, the system incorporates eight BrotherHobby LPD 2306.5 2000KV rotors paired with Gemfan 513D 3-blad 3D propellers, two Tekko32 F4 4in1 50A ESCs, and Pixhawk as a flight controller. Position data were captured using external Vicon cameras. Regarding hardware parameters, the rotor time constant is $\alpha_f = 0.07$ s (as shown in Fig. 1), the mass is $m = 1.481$ kg, the moment of inertia matrix is $\mathbf{J} = \text{diag}(0.020, 0.021, 0.020)$ kg·m², and the arm length $\|l_i\| = 0.15$ m. For the control software, we utilized the PX4 Autopilot as a baseline.

The experimental validation consisted of three main test cases: a purely translational trajectory, a single-axis rotational trajectory, and a multi-axis rotational trajectory. These tests were designed to highlight different aspects of how rotor dynamics affect the multirotor's performance in position and attitude control. The last multi-axis rotational test showcased the combined effects on both position and attitude control during aggressive maneuvers.

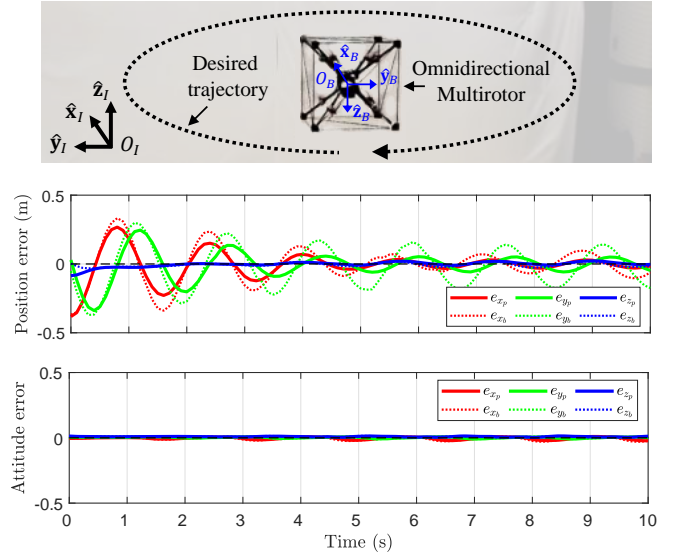


Fig. 4. (M-B): Comparison of the omnidirectional multirotor's position and attitude error between the proposed and baseline controllers over the purely translational trajectory shown on top. The subscripts p and c indicate the proposed and baseline controllers, respectively. Position error of the proposed method reveals significantly lower transient and steady-state tracking errors in the x and y directions, highlighting the enhanced translational tracking performance.

A. Tracking a Purely Translational Trajectory

The multirotor tracks a circular trajectory: $0.4 \sin(\pi t)$ m. The desired height is fixed at 1 m. To exclude the impact of rotational dynamics on the translational system, we set the desired attitude $\mathbf{R}_d = \mathbf{I}$. This trajectory allows us to exclude rotational dynamics while examining the performance of the translational controller.

Figure 4 presents the results of this experiment, illustrating the superior tracking performance of the proposed controller along the \hat{x}_I and \hat{y}_I axes. Unlike the baseline controller, which exhibits significant tracking errors in these axes due to its inability to counteract the effect of rotor dynamics, our controller demonstrates robust compensation capabilities, achieving 32% less position root-mean-squared error (RMSE) compared to the baseline approach. As discussed in Section III, these disturbances are exacerbated by longer rotor settling time (bigger α) and are more pronounced with the translational jerk $\ddot{\mathbf{v}}$ specific to the given trajectory. Both controllers maintain consistent performance along the \hat{z}_I -axis, where a fixed height of 1 meter renders the $\alpha m \ddot{\mathbf{v}}$ in (15) negligible. Similarly, because the desired rotation matrix remains fixed, \mathbf{M} is zero, resulting in comparable rotational tracking performance for both controllers. These results demonstrate the enhanced translational tracking capability of the proposed controller and its ability to mitigate the adverse control effects due to rotor dynamics.

B. Tracking a Single-axis Rotational Trajectory

To validate the rotational control system under the influence of rotor dynamics, particularly focusing on the effects of a high angular jerk, we designed this experiment, which

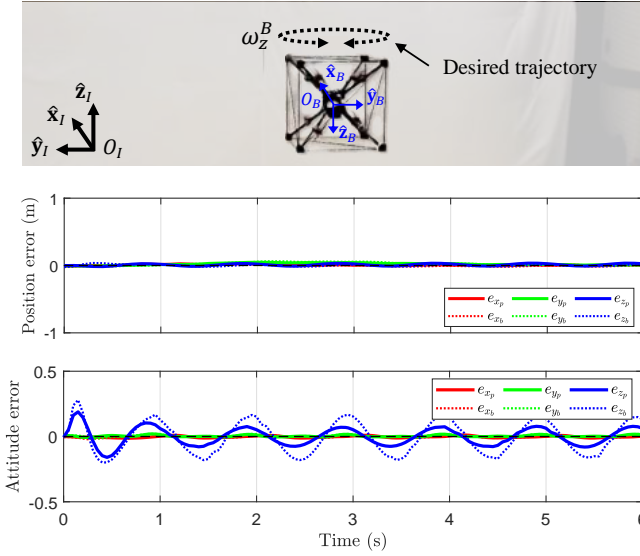


Fig. 5. (M-B): The comparison of position and attitude tracking errors of the omnidirectional multirotor with the proposed and baseline controllers over the purely rotational trajectory shown on top. The proposed controller demonstrates superior attitude tracking performance, particularly around the z-axis where high angular jerk is applied while maintaining comparable positional stability to the baseline controller.

restricts the rotation to a single axis. The platform, initially hovering at position $\mathbf{p}(0) = [0, 0, 1]^T$, followed a desired angular velocity $\omega_z^B = \frac{\pi}{2}(\sin(\pi t))$ rad/s, where the superscripts B indicate the body frame. This trajectory was specifically chosen to generate significant angular jerk, signifying the term $\mathbf{J}\dot{\omega}$ in equation (14), while not exciting other terms induced from rotor dynamics.

Figure 5 illustrates the results of this experiment. The impact of rotor dynamics was prominently observed in the attitude control, particularly around the z_B -axis where the high angular jerk was applied. The baseline controller exhibited significant attitude tracking errors due to its inability to account for the rotor dynamics in the presence of high angular acceleration and jerk. In contrast, the proposed controller demonstrated superior performance, substantially reducing the attitude RMSE by 39%. This marked improvement in attitude control can be attributed to the proposed controller's compensation for the effects of rotor dynamics, particularly the term $\mathbf{J}\dot{\omega}$ in (16). By incorporating these dynamics into the control design, the proposed method was able to anticipate and counteract the disturbance introduced by rotor dynamics, resulting in more precise attitude tracking during the aggressive rotational maneuver. Since the translational dynamics are not directly influenced by an angular jerk and the rotation axis is parallel to gravity resulting in $\mathbf{F} \times \omega = 0$, both controllers maintained similar positional stability throughout the maneuver.

C. Tracking a Multi-axis Rotational Trajectory

We designed a trajectory to signify terms in both translational and rotational dynamics that are impacted by the rotor dynamics, including $\mathbf{F} \times \omega$, $\dot{\omega} \times \mathbf{J}\omega + \omega \times \mathbf{J}\dot{\omega}$, and $\mathbf{J}\dot{\omega}$ shown in (15) and (16). The vehicle followed a desired

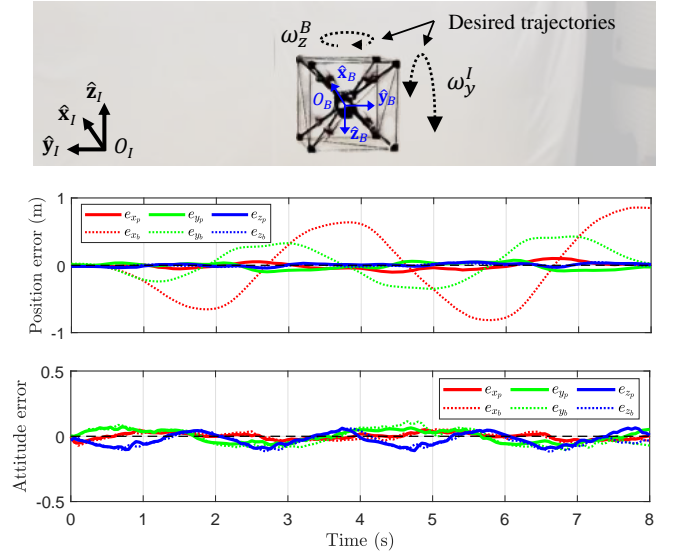


Fig. 6. (M-B): The comparison of position and attitude tracking errors between the proposed and baseline controllers over the multi-axis rotational trajectory shown on top. The proposed controller's position and attitude errors highlight the improved tracking performance of the proposed method in multi-axis rotational motion.

angular velocity $\omega_z^B = 2\pi$ rad/s and $\omega_y^I = \frac{\pi}{2} \sin(\pi t)$ rad/s, where the superscripts I indicate that the vector components are expressed in the inertial frames.

Figure 6 illustrates the results. The baseline controller's position errors are due to rotor settling times. As the platform rotates, delayed rotor response redirects $mg\hat{z}_I$ that was intended for gravity compensation. Consequently, this misalignment results in undesirable forces along the \hat{x}_I -axis and \hat{y}_I -axis, leading to the position error. In contrast, the proposed controller exhibited significantly smaller errors, effectively mitigating these undesirable effects by incorporating rotor dynamics into the control design.

For the attitude controller, despite the aggressive rotational trajectory, the attitude error remained small, validating the $\mathbf{R}^T \mathbf{R}_d \approx \mathbf{I}$ approximation. The proposed controller improved the attitude RMSE by 11%. The relatively modest improvement, compared to significantly impacted positional tracking, can be attributed to the inertia matrix \mathbf{J} being nearly an identity matrix, which rendered the terms $\dot{\omega} \times \mathbf{J}\omega + \omega \times \mathbf{J}\dot{\omega}$ negligible. Furthermore, the complex trajectory triggering simultaneous rotation around all three axes distributed the control efforts, resulting in insufficient angular jerk in any single axis to prominently showcase the effects of rotor dynamics on the control system's performance.

VI. CONCLUSION AND FUTURE WORK

In this paper, we studied the problem of tracking control for omnidirectional multirotors performing aggressive maneuvers, where the rotor dynamics become significant. We designed a novel geometric controller by incorporating a thrust dynamics model for the rotor dynamics, which improves both the positional and rotational control of these systems. The zero equilibrium of the tracking error dynamics

is shown to be almost globally exponentially stable using Lyapunov's direct method. Additionally, we validated the proposed controller's stability and tracking performance in three experiments that highlight different aspects of rotor dynamics' impact on the tracking control.

For future work, the DCMD model can be used in the analysis to characterize the rotor dynamics more accurately than the current thrust model. This would entail a comprehensive analysis involving both simulation and experimental testing to verify and refine the model's accuracy under various environmental conditions. Additionally, integrating adaptive control mechanisms that adjust to changes in rotor characteristics and operational demands might improve the efficacy of the control system.

REFERENCES

- [1] H. Lee et al., "CAROS-Q: Climbing aerial robot system adopting rotor offset with a quasi-decoupling controller," *IEEE Robotics and Automation Letters*, vol. 6, no. 4, pp. 8490-8497, 2021.
- [2] C. Kim, H. Lee, M. Jeong, and H. Myung, "A morphing quadrotor that can optimize morphology for transportation," in *Proc. IEEE/RSJ Int'l Conf. on Intelligent Robots and Systems (IROS)*, Prague, Czech Republic, 2021, pp. 9683-9689.
- [3] Z. Wu et al., " \mathcal{L}_1 adaptive augmentation for geometric tracking control of quadrotors," in *Proc. IEEE Int'l Conf. on Robotics and Automation (ICRA)*, Philadelphia, PA, USA, 2022, pp. 1329-1336.
- [4] R. Mahony, V. Kumar, and P. Corke, "Multirotor aerial vehicles: Modeling, estimation, and control of quadrotor," *IEEE Robotics and Automation magazine*, vol. 19, no. 3, pp. 20-32, 2012.
- [5] S. Rajappa, M. Ryll, H. H. Bühlhoff, and A. Franchi, "Modeling, control and design optimization for a fully-actuated hexarotor aerial vehicle with tilted propellers," in *Proc. IEEE Int'l Conf. on Robotics and Automation (ICRA)*, Seattle, WA, USA, 2015, pp. 4006-4013.
- [6] A. Franchi, R. Carli, D. Bicego, and M. Ryll, "Full-pose tracking control for aerial robotic systems with laterally bounded input force," *IEEE Transactions on Robotics*, vol. 34, no. 2, pp. 534-541, 2018.
- [7] P. Zheng, X. Tan, B. B. Kocer, E. Yang, and M. Kovac, "TiltDrone: A fully-actuated tilting quadrotor platform," *IEEE Robotics and Automation Letters*, vol. 5, no. 4, pp. 6845-6852, 2020.
- [8] M. Ryll, H. H. Bühlhoff, and P. R. Giordano, "A novel overactuated quadrotor unmanned aerial vehicle: Modeling, control, and experimental validation," *IEEE Transactions on Control Systems Technology*, vol. 23, no. 2, pp. 540-556, 2015.
- [9] A. Ollero, M. Tognon, A. Suarez, D. Lee, and A. Franchi, "Past, present, and future of aerial robotic manipulators," *IEEE Transactions on Robotics*, vol. 38, no. 1, pp. 626-645, 2022.
- [10] M. Tognon and A. Franchi, "Omnidirectional aerial vehicles with unidirectional thrusters: Theory, optimal design, and control," *IEEE Robotics and Automation Letters*, vol. 3, no. 3, pp. 2277-2282, 2018.
- [11] M. Hamandi, K. Sawant, M. Tognon, and A. Franchi, "Omni-plus-seven (O7+): An omnidirectional aerial prototype with a minimal number of unidirectional thrusters," in *Proc. International Conference on Unmanned Aircraft Systems (ICUAS)*, Athens, Greece, 2020, pp. 754-761.
- [12] E. Kaufman, K. Caldwell, D. Lee, and T. Lee, "Design and development of a free-floating hexrotor UAV for 6-DOF maneuvers," in *Proc. IEEE Aerospace Conference*, Big Sky, MT, USA, 2014, pp. 1-10.
- [13] M. Kamel et al., "The Voliro omniorientational hexacopter: An agile and maneuverable tilttable-rotor aerial vehicle," *IEEE Robotics and Automation Magazine*, vol. 25, no. 4, pp. 34-44, 2018.
- [14] M. Allenspach et al., "Design and optimal control of a tiltrotor micro-aerial vehicle for efficient omnidirectional flight," *The International Journal of Robotics Research*, vol. 39, no. 10-11, pp. 1305-1325, 2020.
- [15] S. Park, J. Her, J. Kim, and D. Lee, "Design, modeling and control of omni-directional aerial robot," in *IEEE/RSJ International Conference on Intelligent Robots and Systems (IROS)*, Daejeon, Korea, 2016, pp. 1570-1575.
- [16] S. Park et al., "ODAR: Aerial manipulation platform enabling omnidirectional wrench generation," *IEEE/ASME Transactions on Mechatronics*, vol. 23, no. 4, pp. 1907-1918, 2018.
- [17] D. Brescianini and R. D'Andrea, "Design, modeling and control of an omni-directional aerial vehicle," in *Proc. IEEE Int'l Conf. on Robotics and Automation (ICRA)*, Stockholm, Sweden, 2016, pp. 3261-3266.
- [18] D. Brescianini and R. D'Andrea, "An omni-directional multirotor vehicle," *Mechatronics*, vol. 55, pp. 76-93, 2018.
- [19] E. Dyer, S. Sirouspour, and M. Jafarinasab, "Energy optimal control allocation in a redundantly actuated omnidirectional UAV," in *Proc. IEEE Int'l Conf. on Robotics and Automation (ICRA)*, Montreal, Canada, 2019, pp. 5316-5322.
- [20] M. Faessler, D. Falanga, and D. Scaramuzza, "Thrust mixing, saturation, and body-rate control for accurate aggressive quadrotor flight," *IEEE Robotics and Automation Letters*, vol. 2, no. 2, pp. 476-482, 2017.
- [21] G. J. Leishman, *Principles of Helicopter Aerodynamics with CD Extra*. Cambridge, England: Cambridge Univ. Press, 2006.
- [22] P. Pillay and R. Krishnan, "Modeling, simulation, and analysis of permanent-magnet motor drives. II. The brushless DC motor drive," *IEEE Transactions on Industry Applications*, vol. 25, no. 2, pp. 274-279, 1989.
- [23] T. Lee, M. Leok, and N. H. McClamroch, "Geometric tracking control of a quadrotor UAV on SE(3)," in *Proc. IEEE Conference on Decision and Control (CDC)*, Atlanta, GA, USA, 2010, pp. 5420-5425.
- [24] H. Jafarnejadsani, D. Sun, H. Lee, and N. Hovakimyan, "Optimized \mathcal{L}_1 adaptive controller for trajectory tracking of an indoor quadrotor," *Journal of Guidance, Control, and Dynamics*, vol. 40, no. 6, pp. 1415-1427, 2017.
- [25] T. Lee, "Exponential stability of an attitude tracking control system on SO(3) for large-angle rotational maneuvers," *Systems & Control Letters*, vol. 61, no. 1, pp. 231-237, 2012.
- [26] Spitzer, A. and Michael, N., "Rotational error metrics for quadrotor control," *arXiv:2011.11909*, 2020.
- [27] G. Strang, *Linear Algebra and Its Applications*. Belmont, CA, USA: Thomson, 2006.
- [28] H. K. Khalil, *Nonlinear systems*. Upper Saddle River, NJ: Prentice Hall, 2002.